DOI: 10.1021/ma100113k

Macromolecules
ARTICLE

Two Competing Crystallization Modes in a Smectogenic Polyester

Barbara Heck,[†] Ernesto Perez,*[,‡] and Gert Strobl*[,†]

[†]*Physikalisches Institut, Albert-Ludwigs-Universität Freiburg, 79104 Freiburg, Germany, and* [‡]*Instituto de Ciencia y Tecnologia de Polimeros, CSIC, 28006 Madrid, Spain*

Received January 15, 2010; Revised Manuscript Received March 18, 2010

ABSTRACT: The work concerns a polyester composed of heptamethylene-bibenzoate units and heptamethylene-terephthalate co-units that has unusual crystallization properties. Nucleation and growth of spherulites competes with a crystal formation within first formed smectic domains. X-ray scattering experiments carried out simultaneously in the ranges of small, intermediate, and wide angles provide detailed information about the structural development in the two different modes. Varying the temperature in time-resolved measurements shows a change in dominance: At high temperatures, only spherulite growth is observed; at low temperatures, the system uses the two-step process via the smectic phase. Sample heating is usually accompanied by extensive reorganization processes, which all end with a final melting at 140 °C; higher melting points are only obtained for crystallization temperatures above 130 °C. Results are presented in the framework of a crystal thickness−temperature nanophase diagram. Data evaluation yields the latent heats of the transitions between the three phases and the macroscopic equilibrium phase transition temperatures. Sizes and annealing properties of crystallites grown in the spherulitic mode obey the laws established for common polymers. The size of the crystallites formed out of the smectic phase varies inversely with the supercooling below the temperature of the smectic−crystalline phase transition.

1. Introduction

Polymerization of units with nematogenic or smectogenic properties leads to liquid crystal (LC) polymers. They combine the characteristic properties of liquid crystals and polymers:[1] A nematic or smectic phase is formed prior to crystallization and, as always in polymers, crystallization remains uncomplete. The final solid state is semicrystalline. It is a special advantage that LC polymers can be uniformly oriented by application of mechanical force in the LC phase. In this way, high degrees of orientation are achieved, which is used in the production of high modulus fibers.[2]

Bello, Perez, and coworkers investigated within this class of materials, in particular, polyesters of bibenzoic acids.[3,4] If the internally stiff groups are separated by all-methylene spacers, then cooling the melt usually leads first to a smectic phase, before crystallites develop in a second step.[5−8] Modifications are achieved by inclusion of therephthalate counits in the chain. As reported recently, an especially interesting behavior is observed for a sample with 10% of therephthalate units. Here a passage through a smectic phase prior to crystallization is not always found. Crystallization also takes place directly if the cooling rate is low or the temperature of an isothermal crystallization is sufficiently high.[9] This opened the possibility of comparing in studies of one sample the usual crystallization mode of polymers with a crystal formation out of a smectic phase. The results were discussed on the basis of the Ostwald rule of stages,[10] which states that a phase transformation will proceed through metastable states whenever they exist. Keller and coworkers had made use of this rule in discussions of the mechanism of polymer crystallization.[11−13] Monotropic liquid crystalline phases in nematogenic or smectogenic polymers, which are passed through only on cooling, are representatives of such metastable states.[13,14]

We continued the work of our previous communication and present now the results of a comprehensive investigation of the structure formation processes in a similar systems, a copolymer with 20% of therephthalate units. The solidification process under isothermal conditions was analyzed over a wide range of temperatures. In addition, the structural changes during heating to the melt were followed. Analysis was based on time- and temperature-dependent X-ray scattering experiments in the small, intermediate, and wide-angle range and was complemented by optical microscopy and differential scanning calorimetry. Heats of transition between the three phases were measured, and sizes of smectic domains and nanocrystallites were determined. We provide a description of the temperature-dependent variations in the framework of a temperature−size nanophase diagram. Crystallization, reorganization, and melting of conventional polymers in bulk are controlled by a set of laws.[15] As it turns out, these laws are again valid for the system under study in the case of direct crystallization. As will be pointed out, crystal growth out of the smectic phase is different. It produces smaller crystals whose size varies inversely with the supercooling below the temperature of the smectic−crystalline phase transition.

2. Experimental Details

The chemical structure of the polymer studied in this work is described in Figure 1. It is a copolyester set up of 80% bibenzoate groups and 20% therephthalate groups, both being expanded by heptamethylene spacers. We address it with the short name C7TB4. Synthesis was carried out at the Instituto de Ciencia y Tecnologia de Polimeros in Madrid, following the same route as that for other copolyesters of this group of materials.[16] The chemical composition of the sample was analyzed by ^{13}C NMR spectroscopy in a Varian 300 spectrometer using deuterated chloroform as the solvent at 40 °C. The molecular weight characterization, carried out in a Water Alliance GPCV 2000 size exclusion chromatograph equipped with two detectors using chloroform as eluent at 35 °C, gave the following results: M_n = 9.33 kg/mol, M_w = 25.2 kg/mol, and an intrinsic viscosity of 0.567 dL/g.

*Corresponding authors. E-mail: ernestop@ictp.csic.es (E.P.); strobl@uni-freiburg.de (G.S.).

 Published on Web 04/19/2010

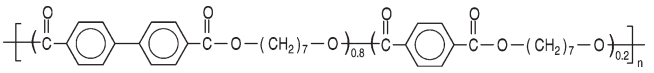

Figure 1. C7TB4, a copolyester composed of 80% heptamethylene-bibenzoate groups and 20% heptamethylene-therephthalate groups.

We used conventional differential scanning calorimeters (DSCs from Perkin-Elmer) for the registration of thermograms and applied an optical polarizing microscope (Zeiss Axioplan) equipped with a heating stage for morphological observations.

X-ray scattering experiments were carried out at the polymer beamline (A2) of HASYLAB (Hamburg, Germany), at the polymer beamline (CRG BM16) of ESRF (Grenoble, France) and with the aid of a small-angle−wide-angle twin Kratky camera in our lab in Freiburg. All of the employed devices allow a simultaneous registration of scattering patterns in the small-angle range and in the range of intermediate angles (with the smectic reflection around $s = 0.6\ \mathrm{nm}^{-1}$) or wide angles (with primary Bragg reflections around $s = 2.2\ \mathrm{nm}^{-1}$).

We used the temperatures given by the controllers in the different heating chambers and made no attempt to calibrate them accurately. Deviations between true and stated temperatures may go up to some degrees.

2.1. Evaluation of X-ray Scattering Data. The evaluation of the small-angle X-ray scattering (SAXS) curves was based on a calculation of the interface distance distribution function (IDF) identical to the second derivative $K''(z)$ of the 1D electron density autocorrelation function $K(z)$. It follows from the scattering intensity distribution $\Sigma(s)$ using the Fourier relationship[17]

$$K''(z) \propto \int_0^\infty [\lim_{s\to\infty} s^4\Sigma(s) - s^4\Sigma(s)] \cos(2\pi sz)\, \mathrm{d}s \qquad (1)$$

Here s denotes the scattering vector $s = 2 \sin \theta_B/\lambda$ (θ_B: Bragg scattering angle; λ: wavelength of X-ray beam).

In all measurements, the crystal thickness, d_c, was derived from the location of the respective peak in $K''(z)$. d_c generally represents a well-defined quantity, opposite to the amorphous intercrystalline regions, which can greatly vary in thickness. Correspondingly, only one peak is usually found in the IDF, and its location gives d_c.

A useful parameter in the analysis of time- or temperature-dependent experiments is the Porod coefficient, P. It determines for two-phase systems the asymptotic behavior of the scattering function to be[18]

$$\lim_{s\to\infty} \Sigma(s) \propto \frac{P}{s^4} \qquad (2)$$

The Porod coefficient is directly related to the interface area per unit volume, O_{ac}, by

$$P \propto O_{ac}(\eta_c - \eta_a)^2 \qquad (3)$$

where η_c and η_a denote the electron densities of the two phases, here referring to crystals and melt. This relation is generally valid for macroscopically homogeneous as well as for macroscopically heterogeneous structures and therefore, for example, also during a spherulitic crystallization or within the melting region.

Prerequisite of a data evaluation based on the IDF is the existence of plate-like crystallites in the sample that are flat over distances distinctly larger than the crystal thickness. This is ensured for crystals in spherulites, and is (according to AFM observations on similar materials[19]) also a plausible assumption for the crystals growing out of a smectic matrix.

Even if polymer crystallites appear in SAXS experiments as being homogeneously extended in lateral direction, they always possess a granular substructure.[15] It shows up in the line width, Δs, of Bragg reflections, which is reciprocal to the coherence length, that is, in our case, the size of the granules, D

$$D = 1/\Delta s \qquad (4)$$

This relationship, known as Scherrer equation, can be used for an estimate of the size of the smectic domains if applied to the line width of the smectic reflection. The Scherrer equation generally relates to the integral width given by the integral reflection intensity divided by the maximum intensity.

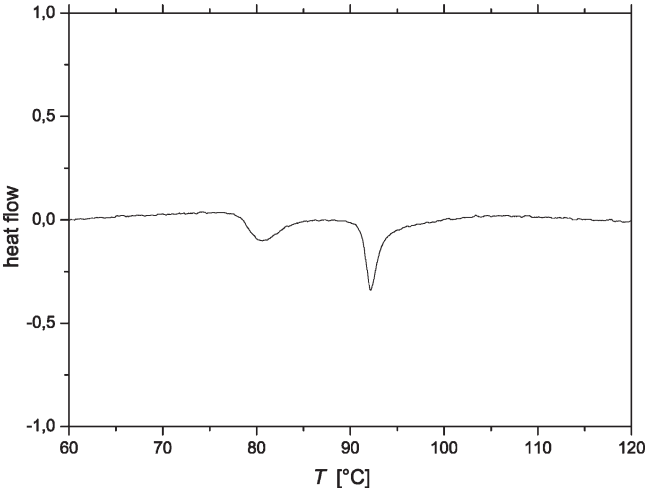

Figure 2. C7TB4 DSC thermogram measured on cooling the melt with a rate of 10 K/min. Two exothermal transitions are observed.

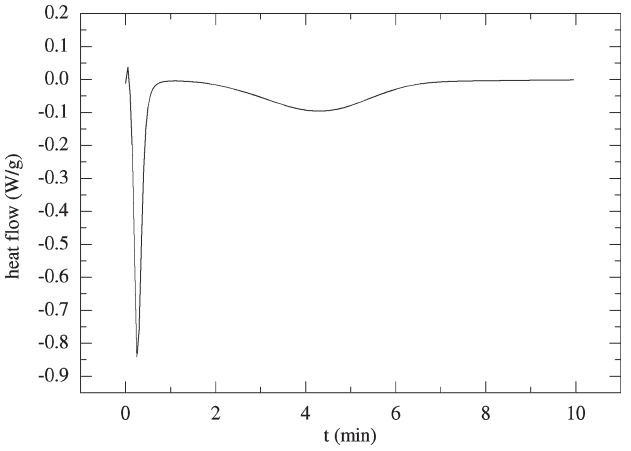

Figure 3. Isothermal solidification at 91 °C: time-dependent DSC curve showing two subsequent transition processes.

3. A First Survey Using Calorimetry and Optical Microscopy

Upon cooling in a DSC a sample of C7TB4 from the melt, two subsequent exothermal transitions are observed, as is shown in Figure 2. The first phase passed through can be thermodynamically stable or, being only kinetically preferred, metastable. A distinction is possible if the solidification process is observed isothermally after a rapid quench to the preset temperature. Figure 3 presents such a DSC isotherm, measured at 91 °C, that is, at the location of the first peak in the thermogram of Figure 2. This first peak appears again, immediately after the quench, but is then followed at a later time by the second transition. Hence, the first transition leads into a phase that is only metastable. The latent heats of the two transition can be determined, and they amount to

$$\Delta H_1 = 11\ \mathrm{Jg}^{-1} \quad \text{and} \quad \Delta H_2 = 18\ \mathrm{Jg}^{-1}$$

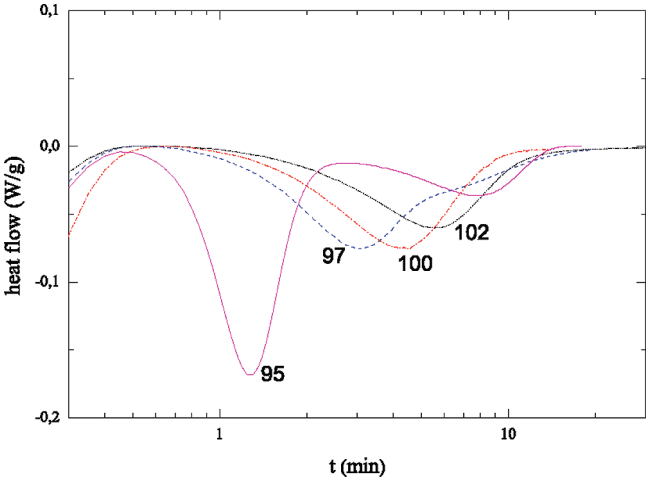

Figure 4. Isothermal solidification at 95, 97, 100, and 102 °C, indicating a change from a two-step to a one-step process.

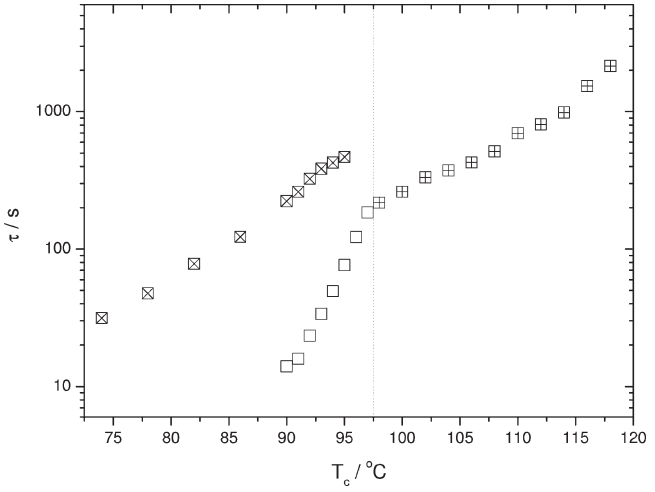

Figure 5. C7TB4: characteristic times of phase transformation as given by the heat flow maxima in DSC isotherms measured at different temperatures. Change from a two-step to a one-step process at 97.5 °C.

Figure 4 collects analogous isotherms as measured at some selected higher temperatures up to 102 °C. For 95 and 97 °C, one still has a two-step process, but then the nature of the transformation changes and a one-step process appears. The characteristic times of the processes, as given by the locations of the exothermal maxima, vary with temperature in the manner shown in Figure 5. All of these times increase exponentially with rising temperature, with different temperature coefficients for the three processes. Observations allow a first conclusion to be drawn: C7TB4 shows two modes of solidification, one corresponding to a two-step and the other to a one-step process. The latter appears for temperatures above 97.5 °C.

Basic structural features of the two modes of solidification show up in time- and temperature-dependent observations in a polarizing optical microscope. Figure 6 presents a temporal series of images taken at four different temperatures after quenches from the melt. At the highest temperature, 114 °C, growing spherulites are observed. At the lowest temperature, 95 °C, the appearance is different. Here a diffuse structure immediately covers the whole view field, and later on, a multitude of small objects develops. At the intermediate temperatures, 99 and 109 °C, both processes are simultaneously active. Hence, we have no sharp transition from a two-step to a one-step solidification process, but a competition between these two modes with a change in dominance.

What is the basic character of the two-step solidification mode? The answer has already been given in the recent report on the solidification behavior of C7TB2, the copolyester with 10% of therephthalate co-units.[9] Here the two-step process has been clearly identified as representing the two steps

$$\text{liquid} \rightarrow \text{smectic phase} \rightarrow \text{crystallites}$$

Being only metastable, the intermediate phase is monotropsmectic. Evidence was provided by the appearance of a smectic reflection in the X-ray scattering pattern prior to the crystal Bragg peaks. Analogous experiments were now carried out for C7TB4, with the results described next.

4. Solidification Processes Analyzed by Time-Dependent X-ray Scattering

Figure 7 presents X-ray scattering curves registered after a quench to 110 °C, that is, during the structure evolution based on the spherulitic crystallization mode. Patterns refer to two different angular ranges. The scattering curves on the right show a section of the wide angle range, which includes the primary crystal Bragg reflections together with the halo of the melt. On the left-hand side, a section at intermediate angles is shown, with a growing reflection at a location related to a period Δz = 1.67 nm. This period corresponds to the length of a monomeric unit. Hence, as to be expected, within the crystals, monomers are arranged in layers, and we find correspondingly a "monomer layer reflection" with Miller index 001. The lamellar crystallites in semicrystalline polymers always possess a granular substructure. The lateral extension of the blocks is to be derived from the line width of Bragg reflections. Application of the Scherrer equation, eq 4, yields here a value of ~20 nm.

Figure 8 depicts the IDFs derived from simultaneously registered SAXS curves. The rising peak with maximum at 7 nm relates to the crystals, and its location gives their thickness, d_c. The minimum that follows yields the long spacing, L = 19 nm. Both lengths are constant in time. The crystallinity within the spherulites, commonly addressed as "linear crystallinity" and denoted α_l, amounts to $\alpha_l = d_c/L = 0.36$. α_l equals the overall crystallinity if at the end of the crystallization process the whole volume is densely filled with spherulites.

Note that the IDF peak, the monomer layer peak, and the Bragg reflections rise simultaneously, as can be anticipated for a solidification processes based on growing spherulites. For the two-step solidification process, this is no longer the case. Figure 9 shows the scattering patterns in the ranges of intermediate and wide angles registered after a quench to 98 °C. Clearly, the monomer layer reflection now appears prior to the crystal Bragg peaks. When the latter begin to rise at a later time, the monomer layer reflection experiences a slight shift to higher angles. Hence, the first step creates longitudinal ordering of the monomers without a regular lateral chain packing; that is, domains with smectic order are formed. In the second step, crystals grow out of the smectic phase. The smectic matrix reacts with some shearing, as is indicated by the slight shift of the reflection position to higher angles.

Evaluation of the simultaneously registered SAXS curves yielded the IDFs depicted in Figure 10. Comparison shows that the IDF peak rises together with the Bragg reflections in Figure 9. The peak location gives d_c = 5.3 nm, and the long spacing minimum is at L = 14.5 nm. Somewhat unexpected, the linear crystallinity is again $\alpha_l = d_c/L = 0.36$, as for the spherulitic mode.

The initial growth of the smectic domains in longitudinal direction can be followed via the time-dependent width, $\Delta s(t)$,

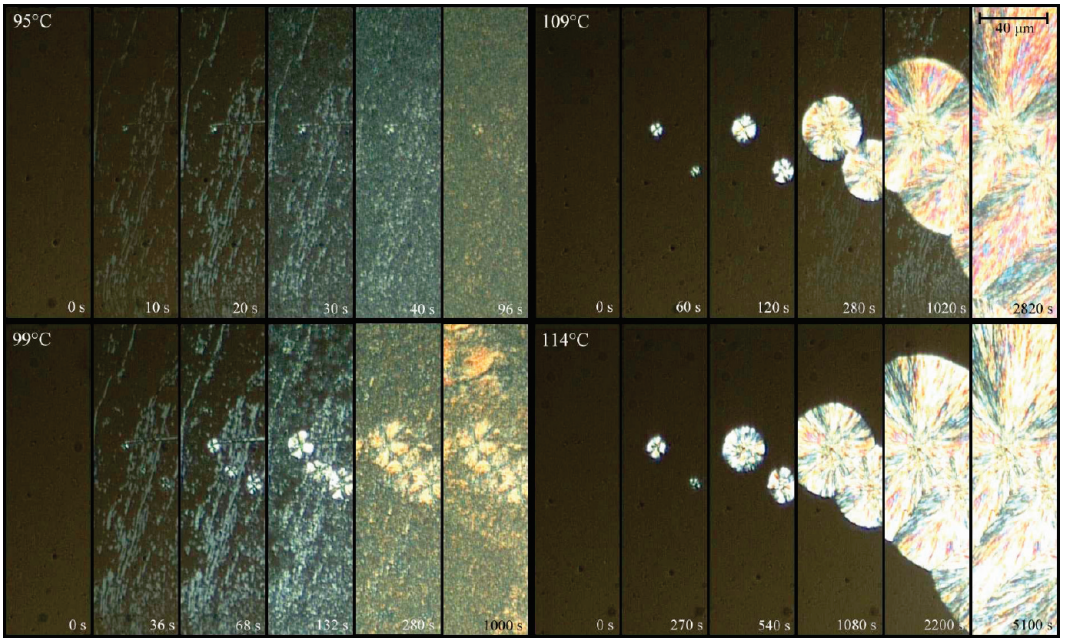

Figure 6. C7TB4, solidication process observed in a polarizing optical microscope: change from a two-step mode via a smectic phase at 95 °C to the growth of spherulites at 114 °C. At 99 and 109 °C, both modes coexist.

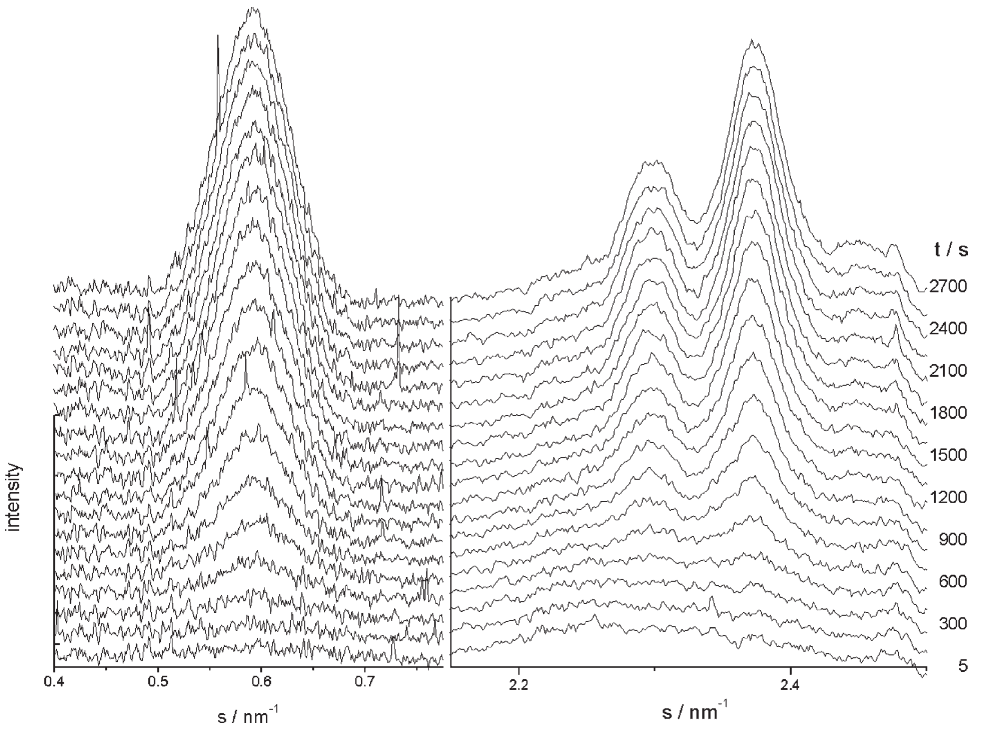

Figure 7. C7TB4 crystallization at 110 °C observed by time-dependent X-ray scattering: simultaneous appearance of a monomer layer peak (left) and crystal reflections (right). The monomer layer thickness as given by the peak location ($s = 0.60$ nm^{-1}) is $\Delta z = 1.67$ nm.

of the monomer layer reflection. Figure 11 shows this dependence in comparison with the constant line width found for the spherulitic mode. In the time range of the experiment, the domain extension rises from 40 (corresponding to $\Delta s = 0.025$ nm^{-1}) to 90 nm. (The maximum around 600 sec is caused by the common appearance of two smectic peaks at slightly different locations at the onset of crystallization.) Crystallization does not change the line width and hence the domain structure. The final domain size, D_{sm}, is much larger than both the crystal thickness and the long spacing. Therefore, we have a state of order in which crystallites are embedded in a smectic matrix. The intercrystalline regions here are smectic and not melt-like as in the usual semicrystalline state. Most probably the sample volume is in the first step completely transferred to the smectic phase; for other smectogenic polyesters, this was demonstrated by NMR spectroscopy.[20] We thus meet here a crystalline−smectic mixed phase without liquid-like regions. For illustration, Figure 12 shows a sketch of this peculiar hybrid structure together with the smectic phase formed in the first step (left). The shift of the smectic peak from $s = 0.584$ to 0.594 nm^{-1} corresponding to a decrease in the

thickness of the monomeric layers from $\Delta z = 1.71$ to 1.68 nm indicates a shearing by ~11°. The block-like crystallites cover 30−40% of the volume. Blocks might be arranged in layers, but a proof would need, for example, AFM imaging.

The spherulitic mode produces as always a crystalline−amorphous structure. The constant line width, $\Delta s = 0.08$ nm^{-1}, observed in this case indicates an extension of longitudinal monomeric order of ~12 nm. This value is larger than the crystal thickness, $d_c = 7$ nm, suggesting that longitudinal order does not end at the crystal surface but is continued over one to two more monomers.

Figure 13 presents in a summary that includes all chosen crystallization temperatures (from 86 to 110 °C in 4 °C steps) the time dependence of three main parameters determined in the isothermal scattering experiments: the integral scattering intensity in the wide angle range, $I_{WAXS}(t)$; the total intensity of the monomer layer reflections, $S(t)$; and the Porod coefficient, $P(t)$.

Especially interesting are the results obtained for 98 °C. The kinetics of the development of the smectic domains and of the subsequent crystallization are separately resolved at this temperature. At lower temperatures, the smectic domains are already present at the beginning of the measurement; at higher temperatures, one observes spherulite growth only.

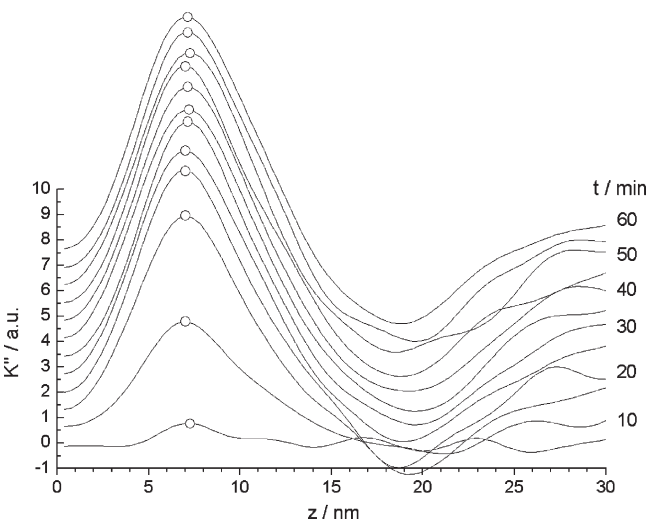

Figure 8. Crystallization at 110 °C. Time-dependent IDFs derived from SAXS experiments. The crystal thickness is $d_c = 7$ nm, the long spacing is $L = 19$ nm, and the linear crystallinity thus amounts to $\alpha_l = d_c/L = 0.36$.

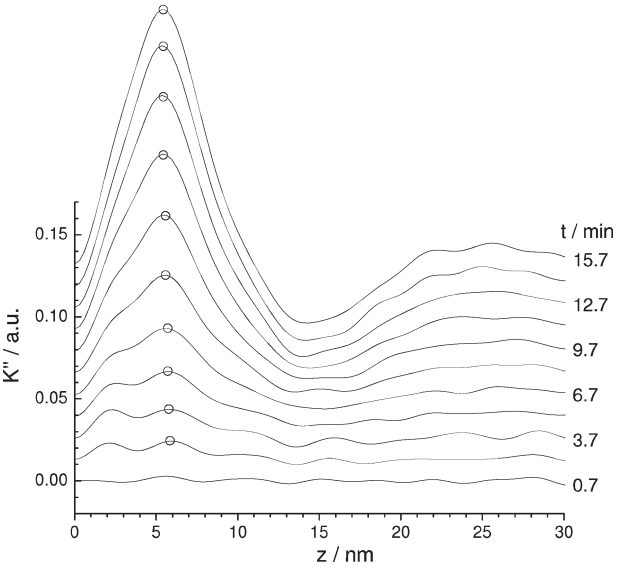

Figure 10. Crystallization at 98 °C. IDFs derived from time-dependent SAXS experiments. The crystal thickness is $d_c = 5.5$ nm, the long spacing is $L = 14.8$ nm, and the linear crystallinity thus amounts to $\alpha_l = d_c/L = 0.37$.

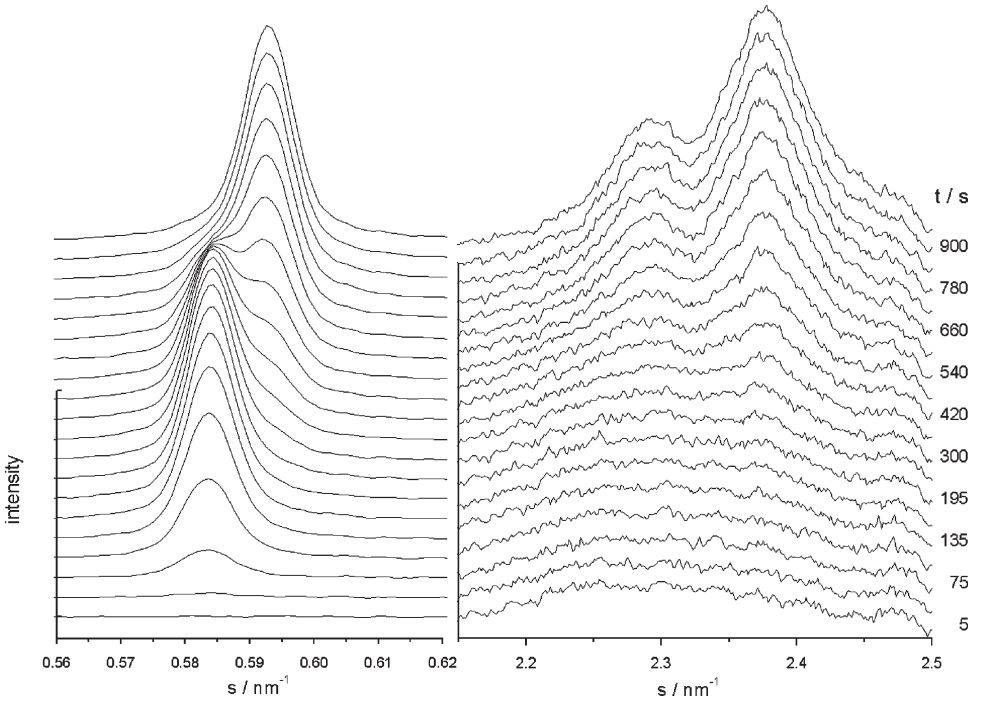

Figure 9. C7TB4 crystallization process at 98 °C observed by time-dependent X-ray scattering at intermediate and wide angles: appearance of a monomer layer peak indicating smectic order (left) prior to the development of crystal reflections (right). Crystal formation out of the smectic phase causes a slight decrease in the smectic period.

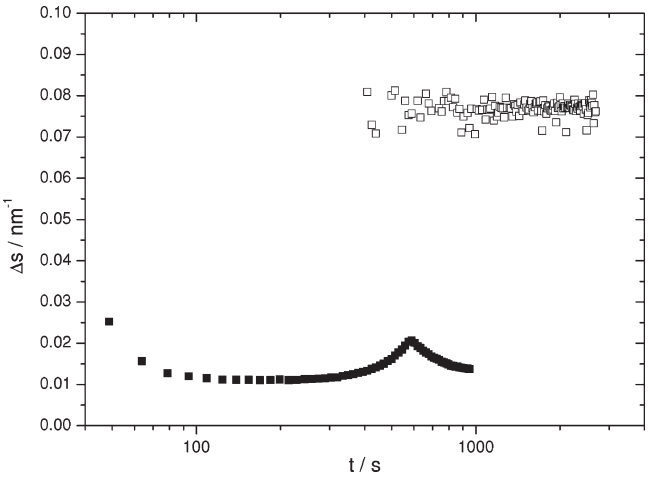

Figure 11. C7TB4 crystallized at 110 (spherulites) (open symbols) and 98 °C (two-step crystallization via smectic phase) (filled symbols): time dependence of the integral width, Δs, of the monomer layer peaks.

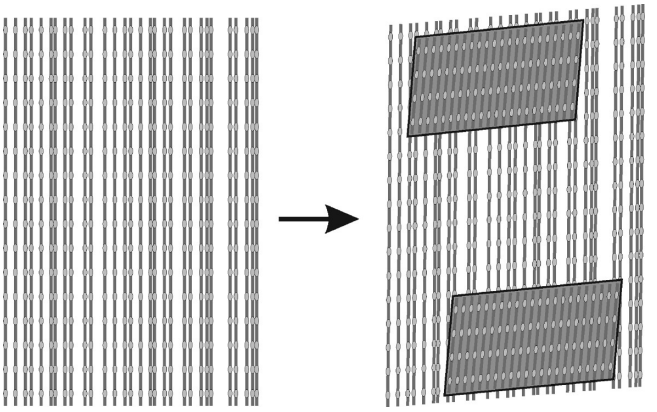

Figure 12. Schematic drawing describing the formation of crystal blocks out of the smectic phase. The initial homogeneous smectic order (period: 1.71 nm) in regions of size 50−100 nm is retained. Crystallites have thicknesses of 3−6 nm and a lateral extension on the order 10 nm; their volume fraction amounts to 0.3 to 0.4. Crystallization induces a weak shear displacement of the chains in the smectic matrix, as is shown by the slight decrease in the smectic period (to 1.66 nm).

The growth of smectic domains at 98 °C obeys the power laws

$$S \propto t^3 \quad \text{and} \quad P(t) - P(0) \propto t^2$$

They are indicative of a 3D growth of a fixed number of smectic domains with constant rate. The values of P in different states can be used for an estimate of the variation of the difference between the densities of melt, smectic matrix, and crystallites. We compare the final values P_1 and P_2 reached for the one- and two-step modes by applying the relationship (from eq 3)

$$\frac{P_2}{P_1} = \frac{O_{sc}(\eta_c - \eta_s)^2}{O_{ac}(\eta_c - \eta_a)^2}$$

η_a, η_s, and η_c denote the (electron) densities of the three phases. O_{sc} and O_{ac} describe the interface areas produced by the two crystallization modes, and these are inversely proportional to the respective long spacings

$$O_{sc} \propto \frac{1}{L_2} \quad \text{and} \quad O_{ac} \propto \frac{1}{L_1}$$

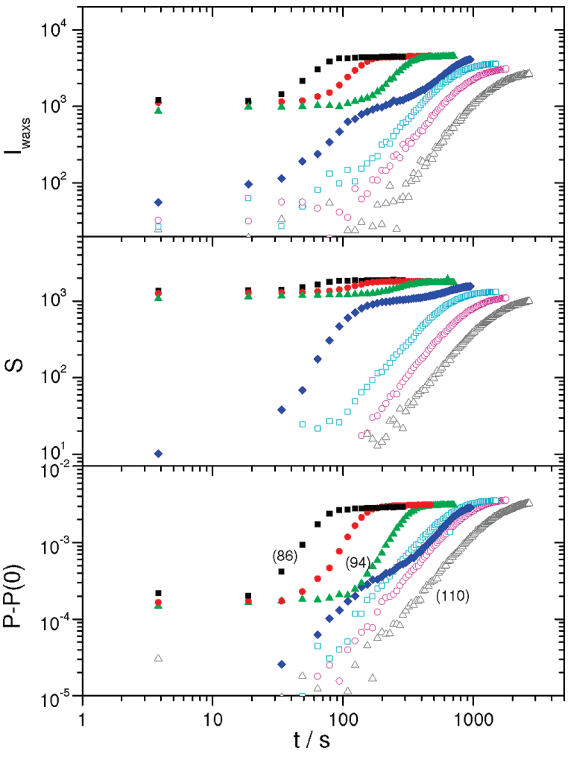

Figure 13. C7TB4 crystallization process at different temperatures studied by time-dependent X-ray scattering in the ranges of small, intermediate, and wide angles: development of the Porod coefficient, P (bottom), of the integral intensity in the range of the monomer layer peak, S (s = 0.514 to 0.662 nm^{-1}) (center), and of the integral intensity in the range of the crystalline reflections, I_{WAXS} (s = 2.253 to 2.476 nm^{-1}) (top).

Insertion of the measured values gives

$$\frac{(\eta_c - \eta_s)^2}{(\eta_c - \eta_a)^2} = \frac{P_2}{P_1}\frac{L_2}{L_1} = 0.79 \times \frac{14.5}{19}$$

leading to

$$\frac{\eta_c - \eta_s}{\eta_c - \eta_a} = 0.77 \quad \text{or} \quad \frac{\eta_s - \eta_a}{\eta_c - \eta_a} = 0.23$$

Such a value is typical for smectic phases.

Considering the two-step process at 98 °C, we find an increase in P by a factor of ~20 from the plateau after the first step to the second plateau. This increase due to the crystal formation is caused by both an increase of the inner surface, which is of the order $D_{sm}/L \approx 6$, and the increasing density difference at the respective interfaces.

5. Heats of Transition and Isotropization Range of the Smectic Phase

We ask about the heat of transition, ΔH_{sa}, and the isotropization temperature, T_{sa}, of the smectic phase. Assuming a complete transformation means to identify the first exotherm in Figure 3 with this latent heat, that is, to set

$$\Delta H_{sa} = \Delta H_1 = 11 \text{ Jg}^{-1}$$

The temperature range of the smectic−liquid phase transition can be determined with the aid of the set of DSC runs shown in Figure 14. After a quench from the melt the sample was kept at 90 °C for the indicated periods of time and then heated. The thermograms change with the annealing time in characteristic

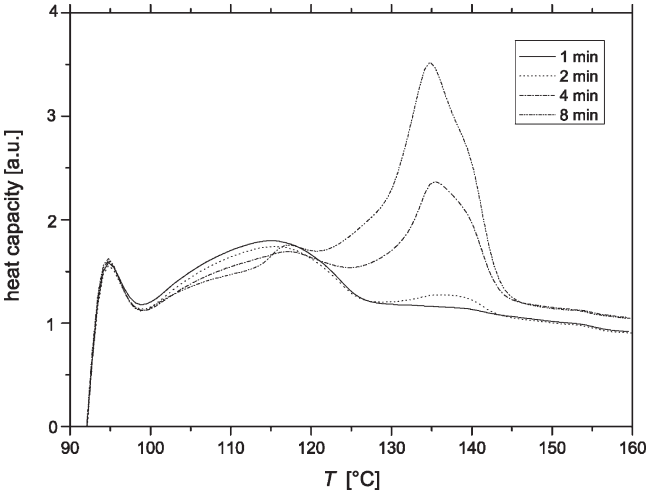

Figure 14. C7TB4 crystallized at 90 °C for the indicated times and then heated with 10 K/min. During the first minute, only the smectic phase forms. Its isotropization range ends at 125 °C. Later on, crystallites develop, which finally melt at 140 °C.

manner. At first, after 1 min of annealing, only one peak appears. Subsequently its magnitude decreases again, and a second peak at higher temperatures shows up. The meaning is clear: the first peak is to be assigned to the isotropization of the first formed smectic phase, and the later appearing broad endotherm relates to the crystal melting. The isotropization of the smectic phase begins already at 100 °C and extends up to 125 °C. Such a broad biphasic region is not unusual for polymeric liquid crystals. It is generally caused by the always present polydispersity, in this case, following from both variations in the counit content and the molar mass.

From the second exotherm in Figure 3 with heat content, ΔH_2, there follows the latent heat associated with the crystallization out of the smectic phase, ΔH_{sc}, as

$$\Delta H_{sc} = \Delta H_2/\alpha_l = 18\ \mathrm{J g^{-1}}/0.36 = 50\ \mathrm{J g^{-1}}$$

The heat of fusion of the crystals thus amounts to

$$\Delta H_{ca} = \Delta H_{cs} + \Delta H_{sa} = 61\ \mathrm{J g^{-1}}$$

The ratio between the heats of transition of the smectic phase and the crystals into the liquid is

$$\Delta H_{sa}/\Delta H_{ca} = 0.18$$

which again compares well with values found for low molar mass smectic LCs.

6. Reorganization and Melting Studied by Temperature-Dependent X-Ray Scattering

Figure 15 presents a series of thermograms registered in a DSC during a sample heating subsequent to isothermal crystallization processes. Crystallization temperatures varied between 74 and 118 °C. Thermograms have a complex appearance, but one feature shows up immediately and allows a straightforward conclusion: the final melting always occurs at the same temperature, 140 °C, independent of the crystallization temperature. This behavior is indicative of extensive reorganization processes, finally leading to the same structure that then melts. Semicrystalline polymers show the same behavior if the crystallization temperature is below a certain point.[15] For the polymer under study, the final melting temperature is even independent of the initial mode of crystallization. This implies a transition from

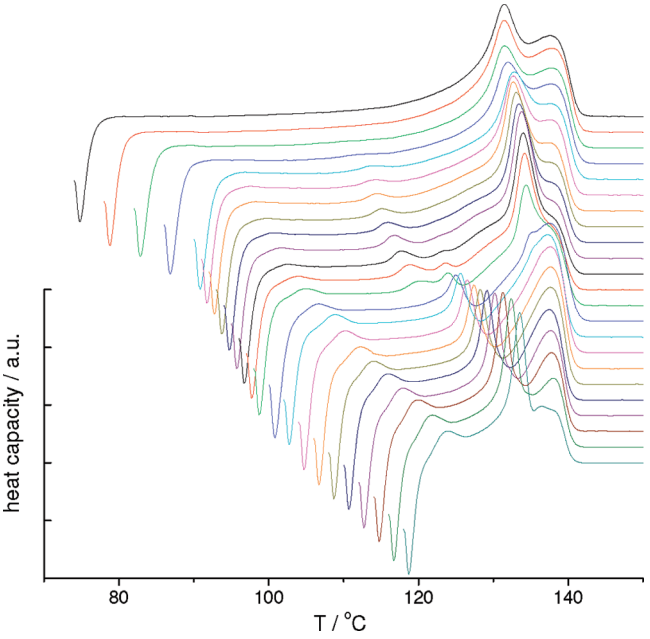

Figure 15. C7TB4 crystallized at various temperatures between 74 and 118 °C and heated with a rate of 8 K/min: DSC thermograms showing the two modes of crystallization with a transfer at about 97 °C. Melting always ends at 140 °C.

reorganization processes via the smectic phase to a crystal reorganization within the amorphous−crystalline state.

What is the nature of the prominent endotherms whose location varies with the crystallization temperature, with a jump at the crossover from one to the other crystallization mode? An assignment is impossible without further insight from other experiments. We carried out temperature-dependent X-ray scattering experiments, both with a stepwise heating in the lab camera and a continuous heating with rates comparable to the DSC at the high brilliance synchrotron radiation sources in Hamburg and Grenoble. At first, we present and consider scattering curves obtained for a sample that was isothermally crystallized at 79 °C. Here crystals are embedded in a smectic matrix, as sketched in Figure 12. Figure 16 depicts three selected scattering patterns recorded in the intermediate range, at the top in the initial state of the completed crystallization at 79 °C and below during heating at 119 and 139 °C. The monomer layer peak has at 79 °C a two-component structure, being composed of two reflections with different width. Exactly such a composite character is to be expected for the structure sketched in Figure 12 with crystallites embedded in a smectic domain. Both the crystallites and the smectic domain possess monomer layer order, extending over about 5−7 nm and 50−100 nm respectively. Correspondingly, the two peaks greatly differ in width. The assignment of the two components is confirmed by the temperature-dependent changes in their intensities. At 119 °C, we still find both of them, but in the scattering pattern recorded at 139 °C, near the final melting, only the crystal component is left. This is understandable because 139 °C is far above the end of the isotropization of the smectic phase (125 °C).

Figure 17 collects the results of all measurements carried out during the heating, giving for both components the integral intensities, *I*. The intensity of the smectic matrix component begins to decrease at 105 °C and vanishes at 130 °C, which is in agreement with the first thermogram in Figure 14. The crystal component keeps a constant intensity up to 130 °C; then, the intensity drops and reaches zero at 145 °C, also in agreement with the DSC observations. (See the remark at the end of Section 2 concerning possible temperature deviations in the cameras.)

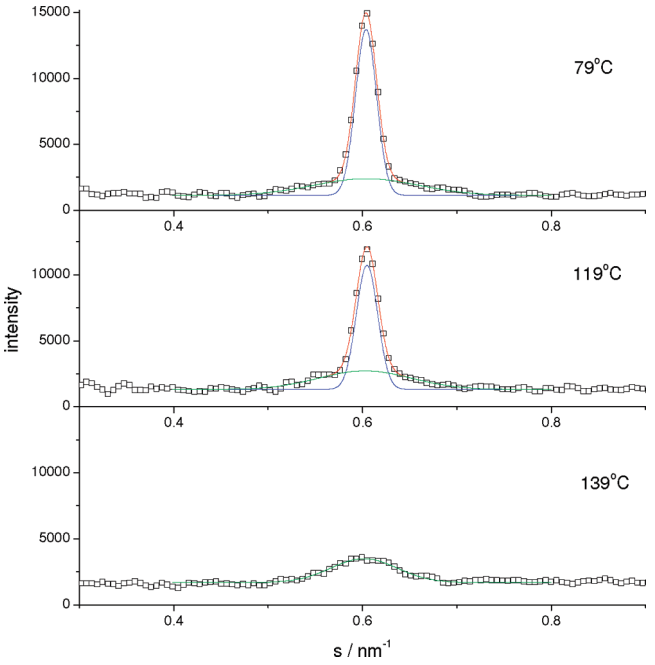

Figure 16. C7TB4 crystallized at 79 °C, followed by a stepwise heating corresponding to a rate of 0.3 K/min. Scattering patterns in the intermediate range obtained at 79, 119, and 139 °C. The narrow component is to be associated with the smectic domains; the broad component relates to the crystallites.

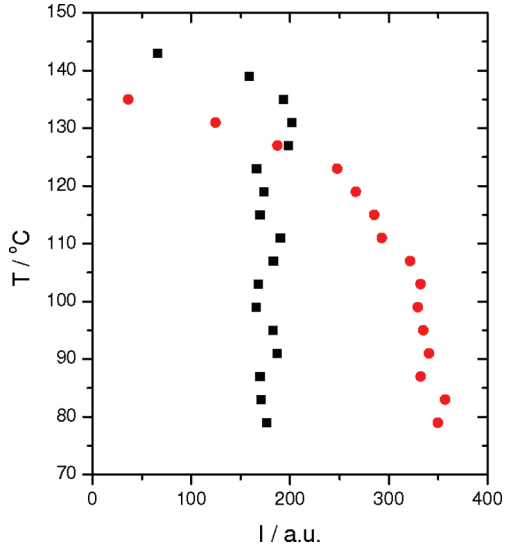

Figure 17. C7TB4 crystallized at 79 °C, followed by a stepwise heating: temperature dependence of the integral intensity I of the narrow (●) and the broad (■) component, respectively.

The simultaneously recorded SAXS curves indicate a crystal thickening. Figure 18 presents IDFs deduced from the data obtained for the initial crystallization at 79 °C. The crystal peak appears at first at a constant location, corresponding to an initial thickness, d_c = 4 nm. At about 107 °C, it begins to shift continuously to higher values, indicating the onset of a continuous crystal thickening. This ends at ∼127 °C, where a jump-like thickness increase is observed. Between 107 and 127 °C, the reorganization of the crystal system obviously takes place within the smectic matrix; that is, a transition of the crystals back into the smectic phase is followed immediately by their reformation with a slightly higher thickness. This peculiar reorganization processes via the smectic phase comes to an end when the existence

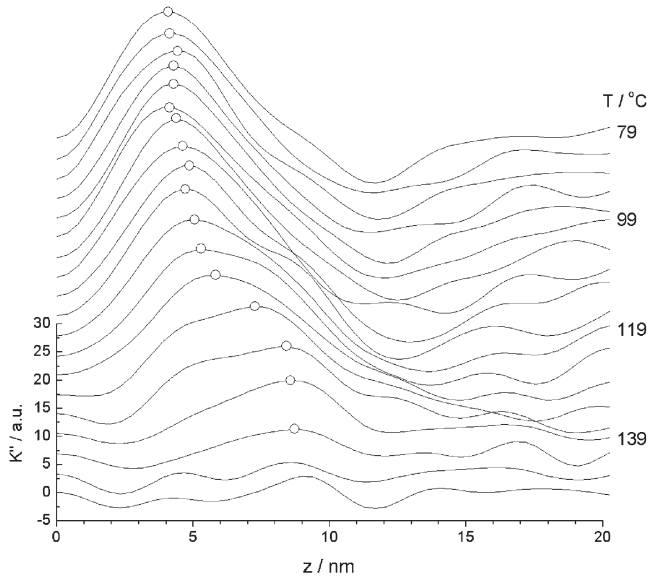

Figure 18. C7TB4 heating after a crystallization from the smectic phase at 79 °C. IDFs derived from temperature-dependent SAXS experiments. Recrystallization processes start at ∼107 °C. The mechanism changes at ∼127 °C, as is indicated by the jump-like increase in the crystal thickness.

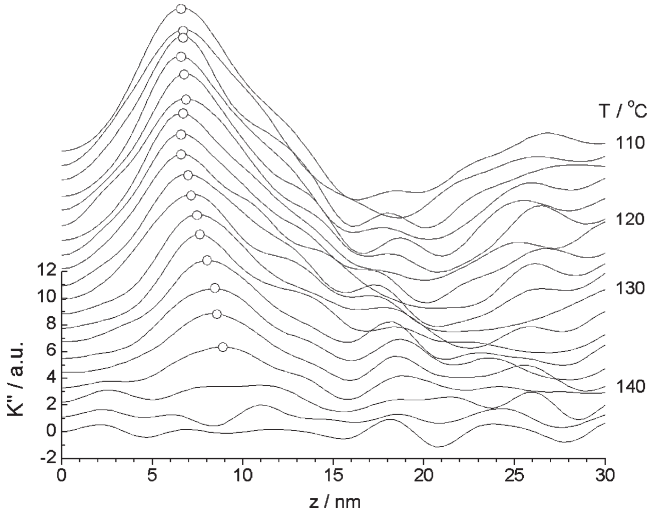

Figure 19. C7TB4 heating after a crystallization at 110 °C. IDFs derived from temperature-dependent SAXS experiments. Reorganization processes set in at 126 °C.

range of this phase is left. Important to note, reorganization then still continues to final melting at 140 °C but now within the other regime, which does not make use of the smectic phase.

Figure 19 shows IDFs derived from a temperature-dependent SAXS experiment for a sample that was at first crystallized at 110 °C in the spherulitic mode. The peak location, at first at d_c = 7 nm, remains fixed up to ∼126 °C. Then, a continuous crystal thickening sets in and goes on until the final melting at 140 °C. Only one reflection is found in the range of the monomer layer reflections with a line width comparable to that of the broad component in Figure 16. Melting is associated with a vanishing of this reflection.

The spherulitic crystallization can also be carried out at temperatures much above those chosen in the DSC runs of Figure 15. Crystallization times then rise to many hours and days. The IDF derived from the SAXS curve after a crystallization at the highest chosen temperature, 138 °C, yields a crystal

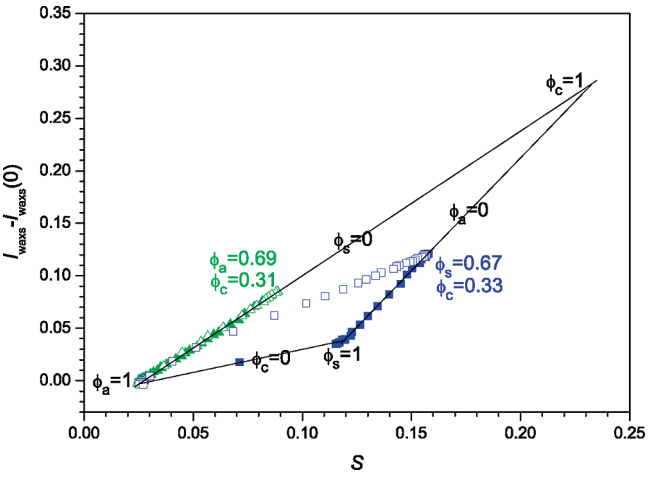

Figure 20. C7TB4 crystallization at 93 (via smectic phase, ■) and 113 °C (spherulites, ▲) always followed by a heating to the melt with a rate of 8 K/min (respective open symbols). Plot of the varying integral WAXS intensity ($I_{WAXS} - I_{WAXS}(0)$) versus the simultaneously measured monomer layer reflection intensity (S). Adjacent points are at a distance of 15 sec (isothermal processes) or 2 K (heating). Each point in the diagram relates to a certain three phase composition ϕ_a, ϕ_s, ϕ_c.

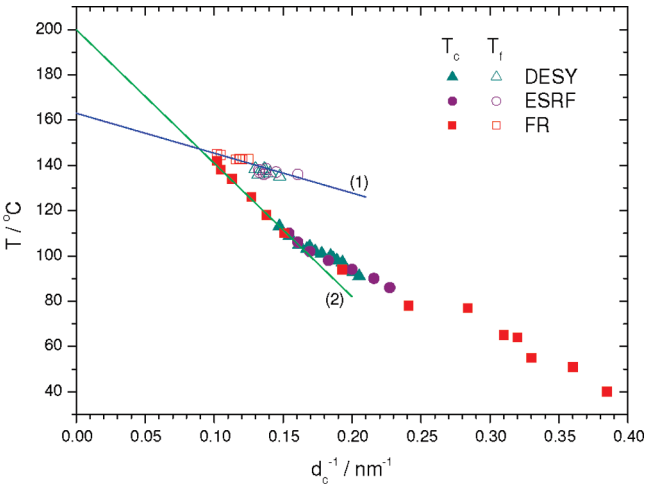

Figure 21. C7TB4 results of SAXS experiments in Hamburg (DESY), Grenoble (ESRF), and Freiburg (FR): variation of the inverse crystal thickness, d_c^{-1}, with the crystallization temperature (T_c, filled symbols) and change of the final melting point with d_c^{-1} (T_f, open symbols). Gibbs−Thomson melting line (1) and crystallization line (2) associated with the spherulitic mode of crystallization.

thickness, d_c = 9.5 nm. In this temperature range, reorganization processes no longer occur, and crystals melt without a prior thickening. Melting is now shifted to 148 °C, which is 8 °C above the final melting of the reorganized crystals. Two temperature ranges of this kind are found for all semicrystalline polymers, with reorganization processes leading to a constant final melting point below a characteristic temperature and absence of thickening together with changing melting points if the crystallization is carried out above this temperature.[21]

In the general case, three phases, fluid, smectic, and crystalline, coexist. One may ask about the composition in a given situation to be described by the three (mass) fractions ϕ_a, ϕ_s, and ϕ_c. Figure 20 demonstrates how this information can be obtained. We plot here the integral intensity in the WAXS range, I_{WAXS} (referred to the initial value in the melt $I_{WAXS}(0)$), versus the intensity of the monomer layer reflection, S, for the following experiments: (1) The filled squares represent the data measured during an isothermal crystallization at 93 °C. The first line up to the break relates to the formation of the smectic domains; the subsequent series of points on a second line results for the crystal formation out of the smectic phase. (2) The following sequence of open squares presents the intensity values measured during the subsequent heating. (3) The sequence of filled triangles allocated on a third line is obtained for a spherulitic crystallization at 113 °C. (4) The points determined during the subsequent heating (open triangles) remain on this line, reaching finally the melt state again.

Each point in this diagrams relates to a certain phase composition, as determined by the linear relationships

$$I_{WAXS} - I_{WAXS}(0) = \phi_a I^a_{WAXS} + \phi_s I^s_{WAXS} + \phi_c I^c_{WAXS} - I^a_{WAXS} \quad (5)$$

$$S = \phi_a S^a + \phi_s S^s + \phi_c S^c \quad (6)$$

with

$$\phi_a + \phi_s + \phi_c = 1 \quad (7)$$

The single phase values I^a_{WAXS}, I^S_{WAX}, and S^a, S^s show up in the two respective lower corners marked ϕ_a = 1 and ϕ_s = 1. The third upper corner assigned to the crystalline state, marked ϕ_c = 1, yields $I_{WAXS}{}^c$ and S^c. It is located at the intersection of two continued lines; the purely crystalline state is not realized in the experiment. The three lines setting up the triangle represent the three possible two-phase states, with the indicated assignments. The diagram can first be used for an estimate of the crystallinities reached at the end of the two analyzed isothermal crystallization processes. Because the crystallinity varies linearly along both the ϕ_s = 0-line and the ϕ_a = 0-line, it can be determined for both the spherulitic crystallization and the crystallization out of the smectic phase. The values thus obtained are 31 and 34%. This agrees within the error limits of the experiment with the linear crystallinities derived from the IDFs (α_l = 0.36). All of the points in the interior of the triangle represent states that include all three phases. Therefore, as to be noted, heating of the initially smectic−crystalline structure produces soon regions with melt. Considering the broad range of the smectic−liquid phase transition (Figure 14), this is to be expected. Simultaneously, the crystal fraction slowly decreases; a trajectory with constant crystallinity would run parallel to the ϕ_c = 0-line, but this is not observed. One may ask about the reason for the difference to the result given in Figure 17, which indicated a constant crystallinity up to the range of final melting. We think the difference is due to the different heating rates, 8 K/min here and 0.3 K/min in the previous case.

6.1. Nanophase Diagram. Macroscopic Transition Temperatures. In numerous investigations on various polymer systems, it was demonstrated that it is appropriate to represent temperature-dependent structure variations within the framework of a d_c^{-1}/T nanophase diagram.[21] In this representation, the laws that control crystallization, reorganization, and melting of bulk polymers become clearly apparent. Figure 21 presents in this manner the inverse value of the crystal thickness found (1) for isothermal crystallization processes at various temperatures between 40 and 141 °C and (2) at the temperature of final melting.

The lower limit of measured melting points, 138−140 °C, relates to all samples that experience a complete reorganization during heating, that is, all of the samples included in the set of DSC curves in Figure 15. Higher melting points are only observed if samples are crystallized at temperatures above 130 °C.

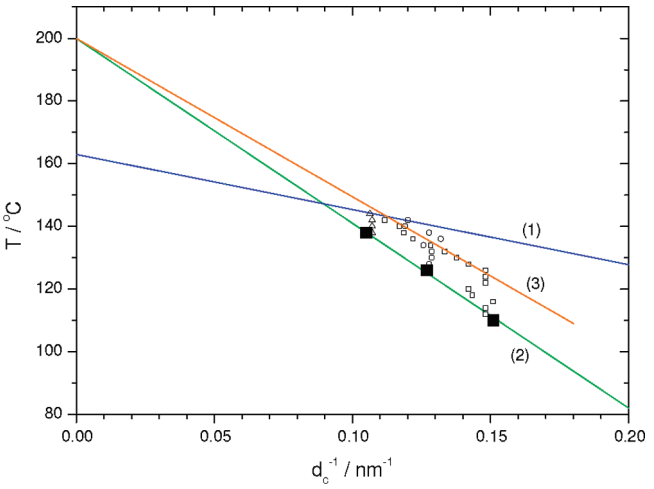

Figure 22. C7TB4 crystallized at 110, 122, and 138 °C and heated stepwise (mean rate: 0.3 K/min). Variation of d_c^{-1} associated with recrystallization processes. Gibbs−Thomson melting line (1) and crystallization line (2) from Figure 21; recrystallization line referring to the spherulitic mode of crystallization (3).

The relationship between d_c^{-1} and the melting point, T, is given by the Gibbs−Thomson equation

$$d_c^{-1} = C_1(T_{ca} - T) \tag{8}$$

C_1 is determined by the heat of fusion and the free energy of the fold surface of the crystallites; T_{ca} denotes the equilibrium melting point of macroscopic crystals. The melting data in Figure 21 can indeed be represented by this "melting line". Its extrapolation to $d_c^{-1} \rightarrow 0$ yields

$$T_{ca} = 163°C$$

Crystal thicknesses resulting from spherulitic crystallization processes at temperatures, T, above 98 °C are determined by the linear relationship

$$d_c^{-1} = C_2(200°C - T) \tag{9}$$

This "crystallization line" is drawn through the respective data in Figure 21. Validity of the equation ends with the crossover to the two-step crystallization mode.

Figure 22 presents the variations of d_c^{-1} during heating processes subsequent to spherulitic isothermal crystallizations at 110, 122, and 135 °C. The sample crystallized at the highest temperature, 135 °C, has a constant thickness up to the melting point; the two other samples experience complete reorganizations. Reorganization processes set in at 125 and 135 °C and then follow a common "recrystallization line", to be described as

$$d_c^{-1} = C_3(200°C - T) \tag{10}$$

The controlling temperature, 200 °C, is the same as that determining the crystallization line. Reorganization processes end at 140 °C, which is the temperature at the intersection of crystallization line and recrystallization line. These results were obtained in the lab camera in a slow stepwise heating process. The onset of reorganization is retarded when higher heating rates are applied, as is possible at the high brilliance synchrotron radiation source in Grenoble. For example, heating with a rate of 8 K min^{-1} after a crystallization at 110 °C resulted in an upward shift of the onset of reorganization by ~5 K.

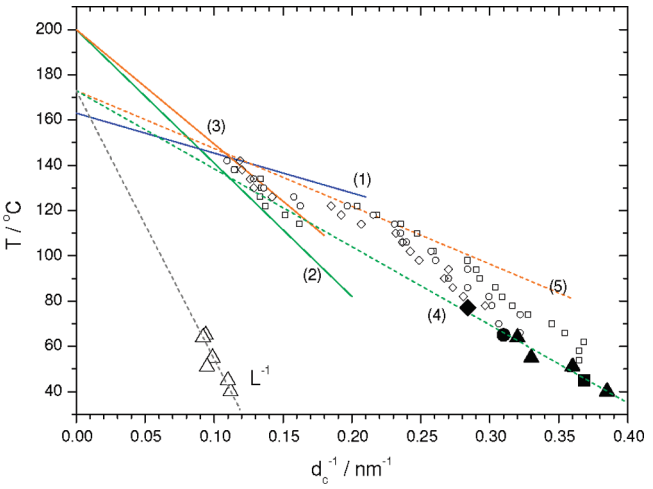

Figure 23. C7TB4 crystallized at several temperatures between 40 and 62 °C, followed by a heating to the melt (rate: 0.3 K/min): variation of the inverse crystal thickness, d_c^{-1}, with temperature. The initial states (filled symbols) are on line (4); recrystallization via the smectic phase follows line (5). Lines (4) and (5) start from T_{sc} = 172 °C. Recrystallization via the smectic phase ends at ~127 °C and is followed by the reorganization process of the spherulitic mode. Long spacings, L, of the initial states change proportional to d_c corresponding to a constant linear crystallinity.

Comparing these observations on crystallization, reorganization, and melting for the spherulitic mode with the general behavior of common bulk polymers, one notes perfect agreement. Behavior is governed as for common polymers by the laws expressed by eqs 8,9, and 10. The laws include different controlling temperatures for the crystal thickness and the melting point. We understand this fact to be indicative of a participation of an intermediate phase in the crystallization process. Crystal growth and also the reorganization processes are supported and accelerated by a passage through such a phase. (See refs 15 and 22 for detailed explanations.) Obviously, this intermediate phase is different from the smectic phase because spherulites grow also at temperatures above the existence range of the smectic matrix.

Which rules govern crystallization and recrystallization of crystals that are embedded in a smectic domain ? Answers are given by the data in Figure 23, which include measurements down to a crystallization temperature of 40 °C:

(1) Both the thickness, d_c, and the long spacing, L, decrease with falling temperature, T, as described by the equation

$$L^{-1} \propto d_c^{-1} = C_4(172°C - T) \tag{11}$$

(2) Crystallites thicken upon heating. For each thickness, there exists an upper stability limit given by the equation

$$d_c^{-1} = C_5(172°C - T) \tag{12}$$

shown in the Figure as line (5). If this limit is reached during a heating process, then the further thickening follows this line.

Reorganization processes within the smectic matrix come to an end at ~125 °C, that is, with the final melting of the smectic phase. Interesting to note, the crossover to the spherulitic mode of crystal growth is associated with a step-like crystal thickening. This holds also in general. Comparison of lines (2) and (4) in the Figure shows that

throughout the existence range of the smectic phase, spherulitic growth would always produce thicker crystals; it does not come true because the two-step mode is here kinetically preferred.

The temperature 172 °C can be understood to be the point of transition between the smectic and the crystalline phase in the macroscopic limit. The crystallites that form at some preset temperature have a size that keeps them just stable. Heating generally leads to a further stabilization by structural improvements and a thickening via the smectic phase. Line (5) represents the locus of transitions of stabilized crystallites into the smectic phase.

At the end of this section, we return to Figure 15 and the question of the assignment of the various peaks in the DSC thermograms. In the first case, we consider the peaks in the spherulite heating and select as an example the peak at 127 °C in the DSC run subsequent to an isothermal crystallization at 106 °C. This can be compared with observations in a corresponding temperature-dependent SAXS run carried out with a similar heating rate, starting from the same initial temperature. The comparison showed that at exactly 127 °C recrystallization processes set in. Upon reaching this temperature, all crystallites soften, that is, get intrinsically mobile. The complete stack of crystallites is reorganized, forming thicker crystals at larger distances. The heat input indicated by the DSC peak means that the reorganization does not fully reproduce the initial crystallinity. The crystallinity drop depends on the heating rate and is much lower or even negligible for the slow stepwise heating used in the lab SAXS camera. Note that reorganization is initiated many degrees before the melting line is reached; the DSC peak is surely not to be associated with a melting of the initial crystallites.

Second, we ask about the nature of the prominent peak before final melting in the thermograms measured for crystallization temperatures below 98 °C when crystals form out of the smectic phase. The peak is generally located in the temperature range 132 to 134 °C, that is, shortly after the disappearance of the smectic phase and the crossover to the spherulitic mode of crystallization. The rapid reorganization via the smectic phase has come to an end and is taken over by the reorganization mechanism of the spherulitic mode. Again, the heating rate is of influence. Whereas the DSC peak indicates a drop in the crystallinity associated with the reorganization, no decrease is seen in the experiment dealt with in Figure 17. At this low heating rate, the crystallinity is mostly preserved up to the final melting.

Third, on heating after a crystallization at 96 °C, a small peak appears in the thermogram at 115 °C. Its assignment follows from the nanophase diagram in Figure 23. At 96 °C, crystals with a thickness $d_c = (1/0.22) = 4.5$ nm develop out of the smectic phase. According to the diagram, the stability end of these crystals as given by line (6) is 115 °C and thus at the location of the DSC peak.

In summary, all endothermal peaks appearing in the DSC thermograms prior to the final melting at 140 °C are to be associated with the onset of reorganization processes. At DSC heating rates, reorganization of the crystal stacks generally leads to a drop of the crystallinity.

7. Phase Thermodynamics and a Data Consistency Check

Dealing with three different phases, melt (index a), smectic phase (s), and crystalline state (c), experiments yielded the following data for the heats and temperatures of transition in the macroscopic limit

$$\Delta H_{sa} = 11\ \mathrm{J g^{-1}}, \quad \Delta H_{ca} = 61\ \mathrm{J g^{-1}}$$

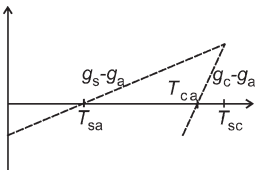

Figure 24. Variation with temperature of the Gibbs free energies, g_s and g_c, of structure units in the smectic and the crystalline phase, referring to the Gibbs free energy, g_a, of the melt.

$$T_{sa} = (273+125)\ \mathrm{K}, \quad T_{ca} = (273+163)\ \mathrm{K},$$
$$T_{sc} = (273+172)\ \mathrm{K}$$

Considering that the isotropization range is broad, T_{sa} is not well-defined, the given value corresponds to the upper limit.

By applying thermodynamics, it is possible to check the data consistency. Figure 24 presents a schematic drawing of the temperature dependencies of the Gibbs free energies g_s and g_c of the smectic and the crystalline phase referring to the Gibbs free energy, g_a, of the melt. The drawing shows the given thermodynamic situation. Because a monotrop-smectic phase is at all temperatures unstable with regard to the crystalline state, T_{sa} has to be located below T_{ca}. T_{sc} is the theoretical point of transition between the smectic and the crystalline phases. It comes to lie above T_{sa} and T_{ca}, hence in a range where both the smectic and the crystalline phase are unstable with regard to the melt. Despite this virtual character, T_{sc} does show up in the experiments as representing the temperature that controls the thickness of the crystallites that grow out of the smectic phase (line (4) in Figure 23).

The scheme implies the equality

$$(g_s - g_a)(T_{sc}) = (g_c - g_a)(T_{sc}) \tag{13}$$

In linear approximation, the slopes of the two drawn lines are given by the standard equations

$$\frac{\mathrm{d}}{\mathrm{d}T}(g_s - g_a) = \frac{\Delta H_{sa} M_m}{T_{sa}} \tag{14}$$

$$\frac{\mathrm{d}}{\mathrm{d}T}(g_c - g_a) = \frac{\Delta H_{ca} M_m}{T_{ca}} \tag{15}$$

M_m denotes the molar mass of the monomer units. This leads to the relationship

$$\frac{\Delta H_{sa}}{T_{sa}}(T_{sc} - T_{sa}) = \frac{\Delta H_{ca}}{T_{ca}}(T_{sc} - T_{ca}) \tag{16}$$

It can be used for a consistency check. Insertion of the data gives for the left-hand side the value 1.30 J g^{-1}, and for the right-hand side, the result is 1.26 J g^{-1}. Hence, the derived data are consistent within the limits of the experiments; regarding the large biphasic region of the isotropization, a perfect agreement would be just accidental. We assumed in the data evaluation a complete transformation of the melt into the smectic phase in the case of the two-step crystallization mode. In addition, linearity was assumed in the extrapolation based on lines (4) and (6) in Figure 23. The essential consistency of the data lends support to both assumptions.

8. Concluding Remarks

Our interest in this polyester composed of smectogenic units arose from its peculiar solidification properties: two modes of crystallization compete, and it is possible to analyze and compare

the different developing structures. One finds a spherulitic mode of crystallization that obeys all of the laws that control crystallization, reorganization, and melting in common polymers and an alternative second mode in which crystallites grow out of first formed smectic domains. Competition between the two modes takes place on the basis of their kinetics. At high temperatures, the liquid−smectic phase transition is much retarded, and the growing spherulites cover a large part of the sample before the transition becomes effective. Oppositely, at low temperatures, the liquid−smectic phase transition is completed before spherulites have nucleated and grow. The crossover from one to the other mode reflects a change in dominance and takes place within a limited temperature range around 100 °C.

Crystallization via the smectic phase creates a specific state whose detailed structure was not analyzed so far. It is still semicrystalline; however, crystallites are now embedded in a smectic rather than a liquid matrix. This hybrid smectic−crystalline state possesses some peculiar properties. Samples show a domain structure, the one formed during the liquid−smectic transition. This structure is preserved when the crystallites form, but the matrix reacts on the crystal formation with a homogeneous shearing. Speculating about the driving force for the shearing one might associate it with the resulting increase in the area of the crystalline−smectic interface. The increase facilitates the transition of chain sequences from the crystalline into smectic regions. It is highly probable, although not proved, that crystallites within a domain have a uniform chain orientation, that which is preset by the smectic director. As it appears, the development of smectic domains is not accompanied by a chain disentangling. Crystallization within the domains is restricted to a fraction of 36%, which is caused by the co-units and also the presence of unresolvable chain crossings, hairpin-turns, and other kinds of entanglements.

The coupling of crystallites to the smectic matrix seems to be stronger than that to fluid surroundings. As shown by Figures 21 and 23, crystallites in contact with the smectic matrix are generally smaller than the crystallites produced by the spherulitic mode of crystallization. In a heating process, they loose their stability when the smectic matrix vanishes at ∼125 °C. We then observe a spontaneous thickening, up to values found for the spherulitic growth regime in this temperature range. Apparently this does not occur as a melting, followed by recrystallization; the nanophase-diagram in Figure 23 indicates that all crystallites developed within the smectic phase have sizes that place them below the Gibbs−Thomson melting line (1). Their size sets them above the recrystallization line (3), that is, outside the stability range of the crystallites in spherulites. Crystallites in this range do not melt, but they are soft and thicken spontaneously. Exactly this reaction is observed.

Acknowledgment. Gert Strobl gratefully acknowledges the support of his work by the Fonds der Chemischen Industrie. The synchrotron work carried out by Ernesto Perez was supported by MEC through specific grants for the access to the CRG beamline BM16 of the ESRF and by the EC Research Infrastructure Action for the access to the soft condensed matter beamline A2 at HASYLAB (program FP6 "Structuring the European Research Area", initiative "Integrating Activity on Synchrotron and Free Electron Laser Science", contract RII3-CT-2004-506008). The inestimable help of the personnel in the two beamlines is greatly acknowledged.

References and Notes

(1) Donald, A.; Windle, H. *Liquid Crystalline Polymers*; Cambridge University Press: Cambridge, U.K., 1992.
(2) MacDonald, W. *Liquid Crystal Polymers*; Elsevier: Amsterdam, 1992.
(3) Perez, E.; Bello, A.; Marugan, M.; Perena, J. *Polym. Commun.* **1990**, *31*, 386.
(4) Perez, E. In *The Polymeric Materials Encyclopedia*; CRC Press: Boca Raton, FL, 1996; Vol. *5*.
(5) Meurisse, P.; Noell, C.; Monnerie, L.; Fayolle, B. *Br. Polym. J.* **1081**, *13*, 55.
(6) Jackson, W.; Morris, J. *ACS Symp. Ser.* **1990**, *435*, 16.
(7) Perez, E.; Marugan, M.; VanderHart, D. *Macromolecules* **1993**, *26*, 5852.
(8) Bello, A.; Perena, J.; Perez, E.; Benavente, R. *Macromol. Symp.* **1994**, *84*, 297.
(9) Fernandez-Blazquez, J.; Perez-Manzano, J.; Bello, A.; Perez, E. *Macromolecules* **2007**, *40*, 1775.
(10) Ostwald, W. *Z. Phys. Chem.* **1897**, *22*, 286.
(11) Keller, A.; Hikosaka, M.; Rastogi, S.; Toda, A.; Barham, P.; Goldbeck-Wood, G. *J. Mater. Sci.* **1994**, *29*, 2579.
(12) Heberer, D.; Keller, A.; Percec, V. *J. Polym. Sci., Polym. Phys. Ed.* **1995**, *33*, 1877.
(13) Keller, A.; Cheng, S. *Polymer* **1998**, *39*, 4461.
(14) Percec, V.; Keller, A. *Macromolecules* **1990**, *23*, 4347.
(15) Strobl, G. *Rev. Mod. Phys.* **2009**, *81*, 1287.
(16) Perez-Manzano, J.; Fernandez-Blazquez, J.; Bello, A.; Perez, E. *Polym. Bull.* **2006**, *56*, 571.
(17) Ruland, W. *Colloid Polym. Sci.* **1977**, *255*, 417.
(18) Strobl, G. *The Physics of Polymers*, 3rd ed.; Springer: Heidelberg, Germany, 2007; p 490.
(19) Hu, Y.; Hiltner, A.; Baer, E. *Polymer* **2006**, *47*, 2423.
(20) Martinez-Gomez, A.; Perez, E.; Bello, A. *Polymer* **2006**, *47*, 2080.
(21) Strobl, G. *Prog. Polym. Sci.* **2006**, *31*, 398.
(22) Strobl, G. *Eur. Phys. J. E* **2000**, *3*, 165.